J Mater Sci (2008) 43:7102–7114
DOI 10.1007/s10853-008-3024-0

# A model kinetics for nucleation and diffusion-controlled growth of immiscible alloys

**Massimo Tomellini**

Received: 3 July 2008 / Accepted: 26 September 2008 / Published online: 24 October 2008


**Abstract** A system of mean field rate equations is employed for describing the kinetics of solid-solid phase separation within the immiscibility gap of binary alloys. The system allows us to study the time evolution of both supersaturation and diffusion length of the components in the metastable phase. It is shown that in the case of simultaneous nucleation the system of differential equations leads to a simple formula for the characteristic time of the transformation in terms of material parameters and initial supersaturation. The nucleation rate is computed on the basis of the classical nucleation theory and the alloy is assumed to behave as a regular solution. It turns out that for low values of the initial supersaturation the nucleation process can be considered as simultaneous. It is also found that thermally activated nucleation takes place for supersaturation values lower than about 0.21. The assumption of a concentration-independent diffusion coefficient and the effect of nucleus curvature on interface composition have been analyzed and discussed.

## Introduction

Phase separation is an important topic in materials science since it usually takes place during the production cycle of materials. In fact, the properties of the product depend on its microstructure which, in turn, is affected by the kinetics of the phase transformation. Since the celebrated theoretical works by Kolmogorov Johonson Mehl and Avrami (KJMA) [1–4] concerning the kinetics of phase transitions ruled by nucleation and growth, and the work by Zener on the diffusional growth of spherical nuclei [5], several studies have been performed aimed at a comprehensive study of phase transformations occurring in multicomponent systems ([6–11] and references therein). The kinetics of the nucleus growth, as formulated by Zener, is usually coupled with the KJMA approach resulting in an equation for the time evolution of the volumetric fraction of the transformed phase. It is worth stressing that kinetics other than the KJMA theory have been formulated to account for the non-random distribution of nuclei [12, 13], the shielding effect due to the anisotropic growth [14, 15], and the parabolic growth law [16, 17]. Computer simulations have also been employed for investigating the microstructure of the system, namely the nucleation density and the particle size distribution function [18–21]. In this context it is worth mentioning the works on the primary crystallization of undercooled liquid where the equation originally proposed in Ref. [5] has been employed by considering the time dependent concentration of the parent phase [21, 22]. The non-homogeneous concentration of the diffusing species is shown to lead to non-random nucleation and to "soft" impingement among clusters. Both effects have been studied in detail in Ref. [21].

Liquid–liquid transformations have recently been analyzed by Zhao et al. [23, 24] by using a mean field approach for describing the particle size distribution function and the nucleation rate under non-isothermal conditions. In these works, the steady state concentration profile around each nucleus is computed according to Ref. [25] by means of the diffusion equation proposed in Ref. [26]. Although this approach exploits a steady state approximation, it permits one to study the evolution of the

M. Tomellini (✉)
Dipartimento di Scienze e Tecnologie Chimiche, Università di Roma "Tor Vergata", Via della Ricerca Scientifica, 00133 Rome, Italy
e-mail: tomellini@uniroma2.it

supersaturation during the transition. This modeling entails a time dependent diffusion length that can be determined, together with the nucleus size, by solving a system of mean field rate equations [25]. The system turns out to be particularly manageable in the simultaneous nucleation case.

The present contribution is aimed at modeling solid–solid phase transition kinetics, ruled by nucleation and growth, occurring in the immiscibility gap of two-component alloys. An important system that fits within this category is, for example, the Fe–C alloy where a phase separation can occur that is ruled by the nucleation and growth of ferrite. In this system, the growth is linked to the diffusion of C atoms within the solid matrix. This process has been recognized to be of relevance in materials science and technology, also in connection with the so-called "metal-dusting" phenomenon [27–29].

In the present work, the kinetics developed in Ref. [25] will be solved, for simultaneous nucleation, and the scaling properties of both diffusion length and duration of the transformation investigated in terms of material parameters. This analysis leads to a quite manageable expression that could be useful in dealing with experimental data. Particular attention will be devoted to the nucleation rate as a function of the fraction of the transformed phase. To this end the thermodynamics of the alloy is described in the framework of the regular solution model with pair-wise interactions. This analysis is also relevant in order to establish whether or not the nucleation process can be considered as simultaneous.

## Results and discussion

### Simultaneous nucleation

In this section, we discuss phase transformation in binary alloys governed by simultaneous nucleation, also referred to as site saturation, where all nuclei start growing at the same time and with the same growth law. Nucleus growth is considered to proceed by atom diffusion in the metastable solution where an equilibrium nucleus/solution interface is assumed [30]. By neglecting any surface effect on the concentration of the species at the interface (the Gibbs–Thomson effect will be discussed in section "Effect of the nucleus curvature on interface composition"), the composition of the interface can be directly related to the phase diagram. A schematic representation of the concentration profiles of the $A$ and $B$ components in the proximity of a nucleus and far from it into the parent phase, $c_A^{(0)}$ and $c_B^{(0)}$, is reported in Fig. 1a. The stable phases are designated as $\alpha$ and $\beta$ and both nuclei of these two phases have been represented in the figure. Panel (b) shows the typical behavior of the molar-free energy of the alloy as a function

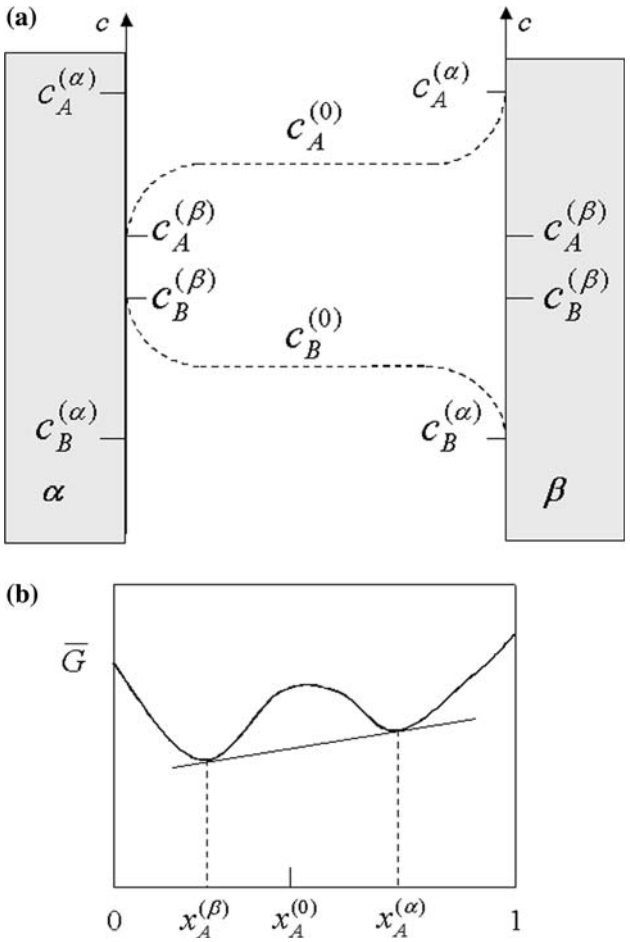


**Fig. 1** **a** Pictorial view of the concentration profile of the two components (designated as $A$ and $B$) of the alloy. The two stable phases, denoted as $\alpha$ and $\beta$, are shown in grey where an equilibrium nucleus/solution interface is considered. $c_A^{(0)}$ and $c_B^{(0)}$ are the concentration of the components far from the interface in the parent phase, $c_A^{(\alpha)}$ and $c_B^{(\beta)}$ the concentration of the two coexisting phases at equilibrium. **b** Isothermal free energy-composition diagram. In the graph the composition variable is the mole fraction of $A$, $x_A$

of composition. The mole fraction of the $A$ component, which is here chosen as the composition variable, is proportional to the concentration according to $x_A^{(i)} = \frac{c_A^{(i)}}{\rho_i}$, where $\rho_i$ is the density of the phase ($i = \alpha, \beta$).

As far as the growth law of the nucleus is concerned, it is usually formulated using the mean field theory. For an interface with infinite mobility [30], the growth rate of a spherical nucleus of the $\alpha$-phase reads [31]

$$\frac{\mathrm{d}R_\alpha}{\mathrm{d}t} = \frac{D_A}{c_A^{(\alpha)} - c_A^{(\beta)}} \left(\frac{\partial c_A}{\partial r}\right)_{r=R_\alpha} = D_A \frac{\sigma_\alpha}{y_\alpha} \tag{1a}$$

where $D_A$ is the diffusion coefficient of $A$, $\sigma_\alpha = \frac{c_A^{(0)} - c_A^{(\beta)}}{c_A^{(\alpha)} - c_A^{(\beta)}}$ the supersaturation, and $y_\alpha$ a characteristic distance defined by the last equality in Eq. 1a. In a like manner, for the formation of $\beta$-phase nuclei, one gets

$$\frac{dR_\beta}{dt} = D_A \frac{\sigma_\beta}{y_\beta}, \tag{1b}$$

with $\sigma_\beta = 1 - \sigma_\alpha$. It is worth stressing that for $y_i = R_i$ Eqs. 1a and 1b give $R_i = (2D_A\sigma_i t)^{1/2}$ where the supersaturation is taken as constant. This last condition has been relaxed in Refs. [21, 22] where Eq. 1 is solved for a time dependent supersaturation, that is $\sigma_\alpha(t) = \frac{c_A^{(0)}(t) - c_A^{(\beta)}}{c_A^{(\alpha)} - c_A^{(\beta)}}$, and at $y_i = R_i$. As far as we know, a mean field approach to the phase transition dealing with characteristic distance ($y$) and supersaturation ($\sigma$), both dependent on time, was first discussed in Ref. [25] by employing the diffusion equation,

$$\frac{\partial c_A}{\partial t} = D_A \left[ \nabla^2 c_A - \frac{c_A - c_A^{(\beta)}}{\lambda_\alpha^2} \right], \tag{2a}$$

where $\lambda_\alpha$ is the characteristic diffusion length and the growth of the α-phase was assumed. Specifically, the last term in Eq. 2a accounts for the depletion of the $A$ atoms this being caused by the growing of the other nuclei located at $r \neq 0$. Integration of Eq. 2a under steady state conditions gives the characteristic distance

$$y_i = \frac{\lambda_i R_i}{\lambda_i + R_i}, \tag{2b}$$

which yields $y_i = R_i$ for $\lambda_i \gg R_i$.

As far as the nucleus growth is concerned, we underline that it is due to the diffusion of both components in the parent phase. The rate of nucleus growth, $\dot{R}_\alpha$, has been expressed in terms of composition and diffusion coefficient of one of the two species, that is component $A$. In fact, the transport of the two components is not independent of each other for, in the diffusion zone, the whole flux of matter is usually assumed to vanish. In the case of a diffusion mechanism mediated by lattice vacancies, this condition ensures that the net flux of vacancy is nil. Furthermore, the mass transport equation (Eq. 2a) holds either for an ideal behavior of the solid solution or for an activity coefficient independent of composition. The validity of this approximation, together with the assumption that no effect is brought about by the curvature of the phase boundary, will be discussed in sections "The thermodynamic factor" and "Effect of the nucleus curvature on interface composition" in the framework of the regular solution model.

In order to solve the kinetics of the phase transformation, Eq. 1 has to be coupled with two more equations representing, respectively, the mass balance and the changing rate of the supersaturation. In particular, the lever rule gives rise to the expression [22, 25]

$$\sigma_\alpha(0) = \sigma_\alpha(t)[1 - X_\alpha(t) - X_\beta(t)] + X_\alpha(t), \tag{3}$$

where $X_i(t)$ is the fraction of transformed phase ($i = \alpha, \beta$), and the density has been assumed to be the same for all the phases.

The connection between the volumetric fraction of the new phase and the nucleus radius is usually established by means of the KJMA theory. Owing to its analytical simplicity, this model has been receiving considerable attention from experimentalists for interpreting kinetic data ([11] and references therein). The validity of the KJMA model in describing phase transformation ruled by diffusion-controlled growth has been analyzed in detail in Ref. [21]. It is shown that owing to the concentration field around the growing nuclei, the spatial distribution of nuclei is non-random, leading to deviation from the KJMA kinetics. In the primary crystallization, this effect has been shown to be negligible relative to the overall kinetics [32].

In the following, we consider the growth of the α-phase only, a hypothesis we will discuss in more detail in the next section, and the KJMA model is employed to estimate the fraction of the transformed phase. Moreover, the nucleation process is considered to be simultaneous, namely nuclei begin to grow at the same time with the same growth law.

By defining the length scale $\overline{d} = N^{-1/3}$, with $N$ being the nucleation density, and the time scale $\tilde{\tau} = \overline{d}^2/D_A$, the system reads

$$\begin{cases} \dfrac{d\rho}{d\tau} = \sigma\left[\dfrac{1}{\eta} + \dfrac{1}{\rho}\right] & 4(a) \\ \dfrac{d\sigma}{d\tau} = -\dfrac{\sigma}{\eta^2} & 4(b) \\ \rho = \left(\dfrac{3}{4\pi}\ln\dfrac{1-\sigma}{1-\sigma(0)}\right)^{1/3}, & 4(c) \end{cases}$$

where $\tau = t/\tilde{\tau}$, $\eta = \lambda/\overline{d}$ and $\rho = R/\overline{d}$ are the non-dimensional quantities and the unnecessary index labeling the phase has been omitted. Numerical integration of the system gives the $\rho(\tau)$, $\sigma(\tau)$, and $\eta(\tau)$ kinetics and, eventually, the fraction of the transformed phase through Eq. 3

$$X(\tau) = \frac{\sigma(0) - \sigma(\tau)}{1 - \sigma(\tau)}, \tag{5}$$

where $X(\infty) = X_\infty = \sigma(0)$. Notably, the system of rate equations (Eq. 4) permits us to evaluate, analytically, the ratio between the nucleus radius and the diffusion length as a function of supersaturation

$$\frac{\rho}{\eta} = \frac{3}{2}(1-\sigma)\left(\ln\frac{1-\sigma}{1-\sigma_0}\right)\left[1 + \left(1 + \frac{4}{3(1-\sigma)\ln\frac{1-\sigma}{1-\sigma_0}}\right)^{1/2}\right], \tag{6}$$

where $\sigma_0 = \sigma(0)$ is the initial supersaturation. The behavior of the function $\eta/\rho$ versus $\sigma/\sigma_0$ is displayed in Fig. 2 for

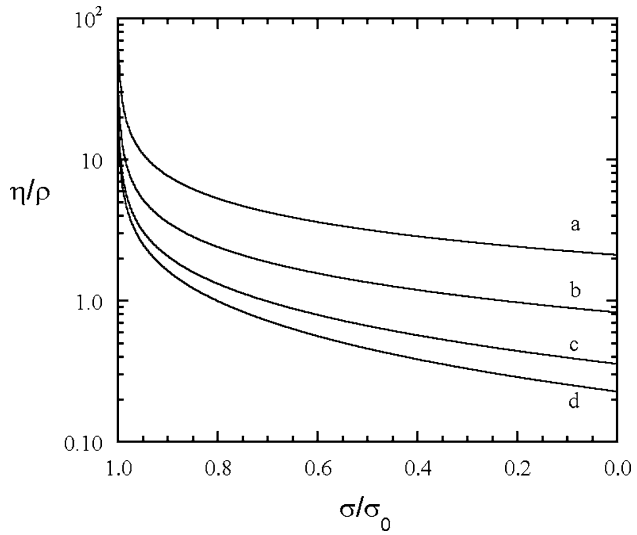


**Fig. 2** Behavior of the ratio between the diffusion length and the nucleus radius as a function of $\sigma/\sigma_0$, for several values of the initial supersaturation $\sigma_0$: (a) $\sigma_0 = 0.05$, (b) $\sigma_0 = 0.2$, (c) $\sigma_0 = 0.5$, and (d) $\sigma_0 = 0.7$. Computations refer to the simultaneous nucleation case

several values of the initial supersaturation. These curves show that the aforementioned assumption, $\lambda = R$, is satisfied during the whole evolution, provided the initial value of the supersaturation is low. Equation 6, together with Eq. 4c, also gives the $\eta(\sigma)$ kinetics that can be used in order to verify the validity of Ham's equation, namely $\frac{\sigma}{\sigma_0} = e^{-K\tau^n}$ where $K$ and $n$ are constants [33, 34]. By inserting these kinetics into the rate equation for the supersaturation (Eq. 4b), the diffusion length is found to scale according to the power law $\eta^{-1} \propto \left(\ln\frac{\sigma_0}{\sigma}\right)^{(n-1)/2n}$. The validity of this assumption has been checked in Fig. 3 where $\eta^{-1}$ has been plotted as a function of $\ln\frac{\sigma_0}{\sigma}$ on double logarithmic scale and for several values of $\sigma_0$. It is found that Ham's equation is satisfied for low values of the initial supersaturation. It is worth noticing that in Fig. 3 the fraction of transformed phase can be easily related to $\sigma' = \frac{\sigma}{\sigma_0}$ by means of Eq. 5 according to $\frac{X}{X_\infty} = \frac{1-\sigma'}{1-\sigma'\sigma_0}$. In the limit $\sigma' \ll 1, \frac{X}{X_\infty} \cong 1 - \sigma'$.

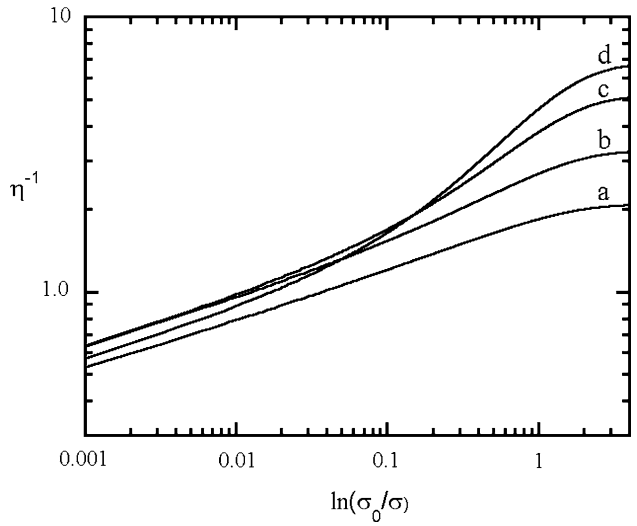


**Fig. 3** Check of the validity of Ham's equation in the case of simultaneous nucleation. In the graph $\eta^{-1}$ has been plotted as a function of $\ln\frac{\sigma_0}{\sigma}$ on double logarithmic scale. Curve (a) $\sigma_0 = 0.05$, (b) $\sigma_0 = 0.2$, (c) $\sigma_0 = 0.5$, and (d) $\sigma_0 = 0.7$. Ham's assumption implies a linear behavior of these plots

The kinetics of the transformed volume are displayed in Fig. 4A, as a function of the dimensionless time $\tau$, and exhibit the sigmoidal-shape typical of phase transitions occurring via nucleation and growth. From these kinetics it is possible to give an estimate of the duration of the transition, $\tau_f$, by assuming the transformation to be completed, say, for $\frac{X}{X_\infty} = 0.95$. The behavior of $\tau_f$ with the initial value of the supersaturation is found to be well described, in the range $0.04 < \sigma_0 < 0.7$, by a power law as shown in Fig. 4B. Therefore, this master plot implies the following scaling of the actual time of the transition,

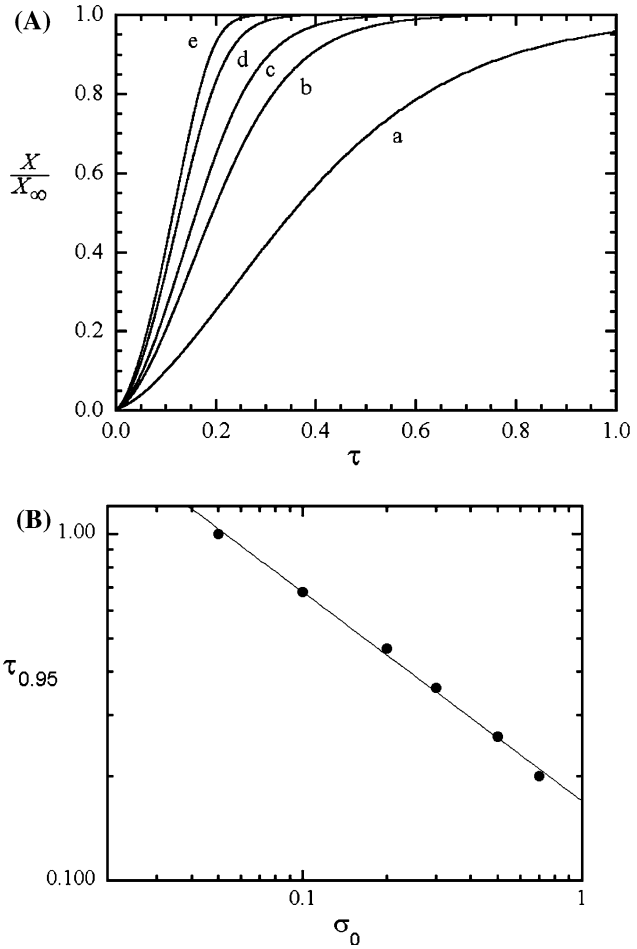


**Fig. 4** **A** Kinetics of phase transformation in the case of simultaneous nucleation for several values of the initial supersaturation: (a) $\sigma_0 = 0.05$, (b) $\sigma_0 = 0.2$, (c) $\sigma_0 = 0.3$, (d) $\sigma_0 = 0.5$, and (e) $\sigma_0 = 0.7$. $X$ is the volumetric fraction of the transformed phase and $\tau$ the dimensionless time. **B** Scaling of the duration of the transition as a function of the initial supersaturation of the solid solution

$$t_f = \frac{C}{\sigma_0^m N^{2/3} D_A}, \tag{7}$$

where $m \cong 0.6$ is the power exponent as derived from Fig. 4B and $C \cong 0.17$.

As far as the concentration profile around a growing nucleus is concerned, it has been computed through Eq. 2 according to [25]

$$\frac{c^{(0)} - c(r')}{c^{(0)} - c^{(\beta)}} = \frac{\rho}{r'} e^{(\rho - r')/\eta}, \tag{8}$$

where $r' = r/\overline{d} \geq \rho$. The behavior of Eq. 8 is illustrated in Fig. 5 for several values of the supersaturation and, therefore, of the nucleus radius. The dimensionless radius and the diffusion length are estimated through Eqs. 4c and 6 for both $\sigma/\sigma_0 = 0.99$ and $\sigma/\sigma_0 = 0.5$ and for several figures of $\sigma_0$. In this context one also observes that since Eq. 3 assumes the concentration to be uniform throughout the sample, it has to be regarded as an approximation, which is more reliable the shorter the range of the concentration field [21].

Strictly speaking, the simultaneous nucleation case is an approximate modeling of the actual nucleation process. Nevertheless, this approach has the merit of permitting a straightforward solution of the kinetics in terms of the more general expression of the characteristic length (Eq. 2b) and allows one to check the validity of the identity $\lambda = R$. Moreover, it gives a simple and direct interpretation of the time needed to complete the transformation in terms of measurable quantities such as supersaturation, diffusion coefficient, and nucleation density (Eq. 7). In the next section, an analysis is presented which is useful in defining the conditions which validate the mean field approach discussed so far.

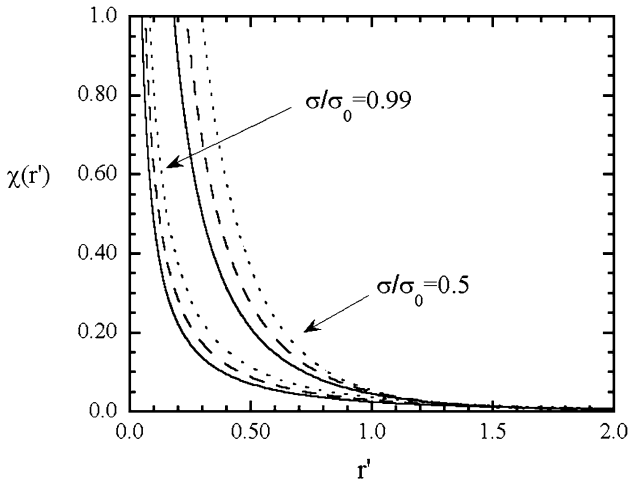


**Fig. 5** Concentration field around a growing nucleus. The behavior of the function $\chi(r') = \frac{c^{(0)} - c(r')}{c^{(0)} - c^{(\beta)}}$ is displayed for $\sigma/\sigma_0 = 0.99$ and $\sigma/\sigma_0 = 0.5$, where $r' = r/\overline{d}$. (*Solid lines*) $\sigma_0 = 0.05$, (*long dashed lines*) $\sigma_0 = 0.1$, (*dashed lines*) $\sigma_0 = 0.2$

Ham's equation can be employed to evaluate the size of the nucleus, at the end of the phase transition, in the case of low supersaturation where the equation has been shown to hold. Since under this circumstance $\rho \ll \eta$, Eq. 4a gives $\rho^2 = \frac{2\sigma_0}{nK^{1-\alpha}} \int_0^w w^{-\alpha} e^{-w} dw$ where $w = \ln \frac{\sigma_0}{\sigma}$ and $\alpha = \frac{n-1}{n}$. Consequently, the maximum size of the cluster is $\rho^2_{\max} = \frac{2\sigma_0}{nK^{1-\alpha}} \Gamma(1-\alpha)$, where $\Gamma(x)$ is the gamma function.

The model discussed so far can be useful for interpreting experimental data on phase separation in binary systems. Specifically, for a given initial composition of the alloy, $x_A^{(0)}$, one considers a sudden temperature change that brings the alloy into the immiscibility gap, i.e. from a one-phase to a two-phase region of the phase diagram. In this case, provided that heat transfer is fast compared with the kinetics of the phase transition, at the end of such a temperature jump the system is still a single phase, namely the metastable solution, with initial composition $x_A^{(0)}$ (Fig. 1b). The model applies to the isothermal phase separation at this final temperature. On the other hand, the metastable phase within the immiscibility gap can be reached, at a given temperature, through variation in composition, as is thought to occur in metal dusting.

Experimental techniques do exist that allow one to measure the $X(t)$ kinetics. These techniques are based, for example, on calorimetric and spectroscopic measurements performed during the transition. The model kinetics presented here highlight the conditions under which experimental data can be safely analyzed in the framework of Ham's law, that is by using Avrami's plot. In this case the fitting parameters, $K$ and $n$, can be linked to the activation energy of the transition and to the growth law of the cluster, respectively, as discussed in detail in Refs. [11, 25]. As an application of the scaling law Eq. 7, let us consider the metal dusting caused by the catalytic reduction of hydrocarbon on the iron surface. As discussed in Refs. [27–29], metal dusting is driven by the phase separation of a metastable Fe–C solid solution in the presence of graphite. The transition is considered to proceed via C-phase nucleation and growth [27, 28]. Furthermore, kinetic measurements have been performed which give the rate constant of the whole process, $K_M$, and its temperature dependence. For the Fe–C system an activation energy of 200 kJ/mol has been reported [27, 28]. Therefore, in an attempt to interpret the temperature dependence of $K_M$ on the basis of the present approach, we identify $K_M^{-1}$ with the length of the transition, $t_f$. Accordingly, one infers that $\frac{2}{3}\Delta H_N^{\#} + \Delta H_D^{\#} \cong 200$ kJ/mol, where $\Delta H_N^{\#}$ and $\Delta H_D^{\#}$ are the activation energies for nucleation and diffusion, respectively.

## Nucleation rate

This section is devoted to modeling the steady state nucleation rate in binary alloys as a function of supersaturation.

This computation is useful in order to check the validity of the two hypothesis commonly employed to deal with this type of phase transition: simultaneous and progressive nucleation. In the former case, the nucleation rate is a Dirac delta function; in the latter, a constant. To this purpose, a thermodynamic approach is developed that is based on the theory of regular solution with pair-wise interactions. The computation pathway implies the evaluation of the free energy change for nucleus formation, which quantity enters the classical theory of nucleation.

According to the theory of regular solution, the molar Gibbs free energy of formation of the alloy is

$$\beta\Delta\overline{G} = \beta\omega\left(\frac{1}{4} - \xi_A^2\right) + \left(\frac{1}{2} + \xi_A\right)\ln\left(\frac{1}{2} + \xi_A\right) + \left(\frac{1}{2} - \xi_A\right)\ln\left(\frac{1}{2} - \xi_A\right), \quad (9)$$

where $\beta = 1/kT$, $k$ is Boltzmann's constant, $T$ the absolute temperature, and $\xi_A = x_A - \frac{1}{2}$, with $x_A$ being the mole fraction of the $A$ component that is the composition variable. In Eq. 9, $\omega$ is related to the excess enthalpy of the alloy that is derived, in terms of pair interactions, according to $\omega = \sum_n z_n\left[\varepsilon_{AB} - \frac{1}{2}(\varepsilon_{AA} + \varepsilon_{BB})\right]_n$, where the sum runs over the coordination shells, $z_n$ is the coordination number, and $\varepsilon_{ij}$ the pair interaction energy. From Eq. 9 it stems that $\Delta\overline{G}$ is an even function of $\xi_A$. Also, by denoting with $\xi = \xi_A^{(\alpha)}$ (assumed here to be greater than zero) the composition of the α-phase and by setting the first derivative of Eq. 9 equal to zero, one gets

$$\beta\omega = \frac{1}{2\xi}\ln\frac{1+2\xi}{1-2\xi}, \quad (10)$$

where $\beta\omega > 2$ holds, since the two-phase region is thermodynamically stable ($0 < \xi < 1/2$). From Eq. 10 it turns out that the $\xi$ parameter completely characterizes the energetics of the system.

The behavior of Eq. 9 is displayed in Fig. 6 as dashed line (right scale). In particular, the two inflection points are located at $\xi_A = \pm\xi_{A,F} = \pm\frac{1}{2}\sqrt{1 - \frac{4\xi}{\ln\frac{1+2\xi}{1-2\xi}}}$ which define the region of the spinodal decomposition ($-\xi_{A,F} < \xi_A < \xi_{A,F}$). Within the spinodal, compositional fluctuations—of wavelength longer than the critical one—grow in amplitude as a function of time yielding to the final product phase. Therefore, the thermally activated process of nucleation does occur in the intervals of composition $\xi_{A,F} < \xi_A < \xi$ and $-\xi < \xi_A < -\xi_{A,F}$. Hereafter the modeling refers to these compositional range.

The chemical potential of the components are estimated through Eq. 9 according to $\mu_A = \mu_A^0 + \Delta\overline{G} + (1 - x_A)\frac{\partial\Delta\overline{G}}{\partial x_A}$ (and similarly for the $B$ component), where $\mu_A^0$ is the

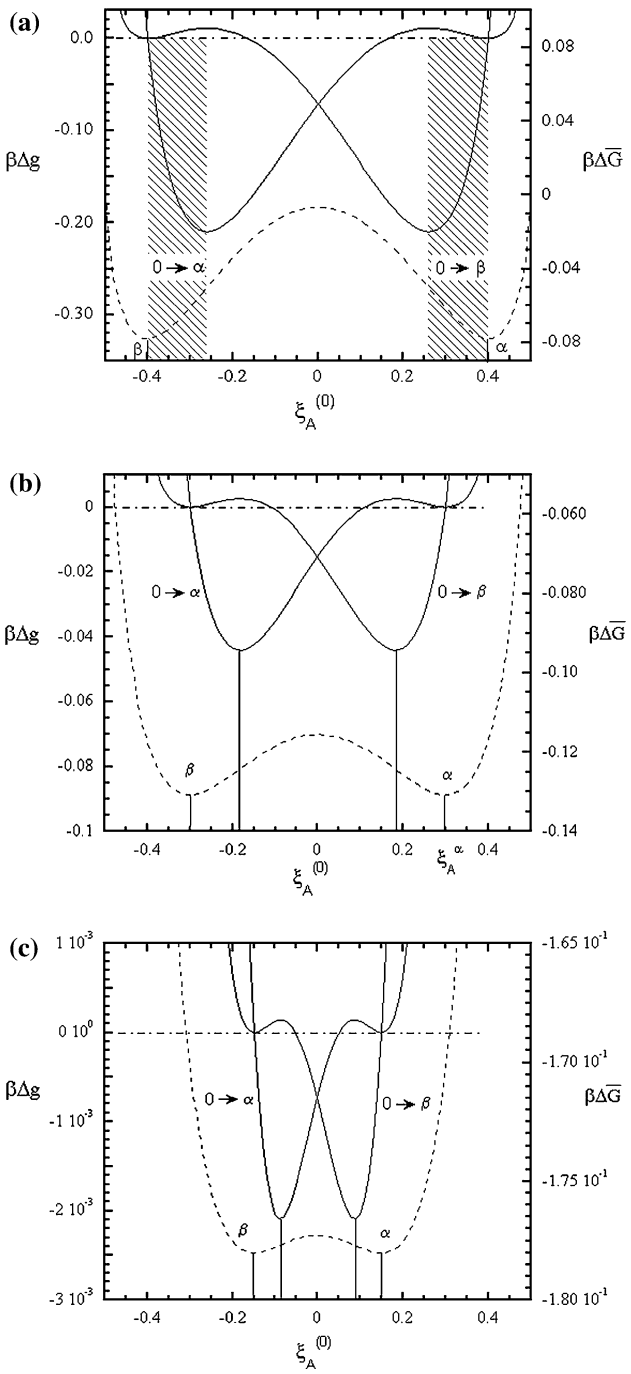


**Fig. 6** "Bulk" contribution to the Gibbs free energy of nucleation as a function of the composition variable $\xi_A^{(0)}$ (*solid lines*, left scale). The computation refers to the formation of both α and β nuclei. In the figure the curves $\Delta g_{0,\alpha}(\xi_A^{(0)})$ and $\Delta g_{0,\beta}(\xi_A^{(0)})$ are labeled as "0 → α" and "0 → β", respectively. The molar free energy of alloy formation ($\beta\Delta\overline{G} \equiv \Delta\overline{G}/kT$) is also shown as *dashed lines* (right scale). The boundaries of the immiscibility gap are located at $\xi_A^{(0)} = \pm\xi_A^{(\alpha)}$ (in the text $\xi_A^{(\alpha)} \equiv \xi$ and $\xi_A^{(0)} \equiv \xi^{(0)}$). **a** The two dashed stripes denote the composition intervals where thermally activated nucleation does occur. Panels **a**, **b**, and **c** refer to $\xi_A^{(\alpha)} = 0.4$, $\xi_A^{(\alpha)} = 0.3$ and $\xi_A^{(\alpha)} = 0.15$, respectively

chemical potential of pure $A$ which is independent of alloy composition. Thus one obtains,

$$\mu_A(\xi_A) = \mu_A^0 + \left(\frac{1}{2} - \xi_A\right)^2 \omega + kT \ln\left(\frac{1}{2} + \xi_A\right) \tag{11a}$$

and

$$\mu_B(\xi_A) = \mu_B^0 + \left(\frac{1}{2} + \xi_A\right)^2 \omega + kT \ln\left(\frac{1}{2} - \xi_A\right). \tag{11b}$$

Let us now move to the computation of the free energy change for nucleation. According to the classical nucleation theory, the free energy for nucleation is given by the sum of "bulk" and "surface" terms. By considering the nucleation of α-phase nuclei, the bulk contribution to the Gibbs free energy, per atom, reads

$$\begin{aligned}\Delta g_{0,\alpha} &= \left[x_A^{(\alpha)}\left(\mu_A^{(\alpha)} - \mu_A^{(0)}\right) + \left(1 - x_A^{(\alpha)}\right)\left(\mu_B^{(\alpha)} - \mu_B^{(0)}\right)\right] \\ &= \left[\left(\frac{1}{2} + \xi\right)\left(\mu_A^{(\alpha)} - \mu_A^{(0)}\right) + \left(\frac{1}{2} - \xi\right)\left(\mu_B^{(\alpha)} - \mu_B^{(0)}\right)\right]\end{aligned} \tag{12}$$

where the index "(0)" designates the metastable solid solution, $\mu_A^{(\alpha)} \equiv \mu_A(\xi_A^{(\alpha)}) = \mu_A(\xi), \mu_B^{(\alpha)} = \mu_B(\xi_A^{(\alpha)}) = \mu_B(\xi)$. A similar expression is obtained for $\Delta g_{0,\beta}$. By inserting Eqs. 11 in Eq. 12 and using Eq. 10 to express $\omega$ in terms of composition, one ends up with

$$\begin{aligned}\beta\Delta g_{0,\alpha}(\xi, \xi^{(0)}) = \Bigg[&\frac{1}{2}\ln\frac{1 - 4\xi^2}{1 - 4\xi^{(0)^2}} + \left(\xi - \frac{1}{2\xi}\left(\xi - \xi^{(0)}\right)^2\right) \\ &\times \ln\frac{1 + 2\xi}{1 - 2\xi} + \xi\ln\frac{1 - 2\xi^{(0)}}{1 + 2\xi^{(0)}}\Bigg]\end{aligned} \tag{13}$$

and

$$\begin{aligned}\beta\Delta g_{0,\beta}(\xi, \xi^{(0)}) = \Bigg[&\frac{1}{2}\ln\frac{1 - 4\xi^2}{1 - 4\xi^{(0)^2}} + \left(\xi - \frac{1}{2\xi}\left(\xi + \xi^{(0)}\right)^2\right) \\ &\times \ln\frac{1 + 2\xi}{1 - 2\xi} + \xi\ln\frac{1 + 2\xi^{(0)}}{1 - 2\xi^{(0)}}\Bigg]\end{aligned} \tag{14}$$

where $\xi^{(0)} \equiv \xi_A^{(0)}$ is the composition of the parent phase. The behavior of these functions is shown as solid lines in Fig. 6a–c for $\xi \equiv \xi_A^{(\alpha)} = 0.4$, 0.3 and 0.15, respectively, together with the curve $\beta\Delta\overline{G}$ (dashed line). As anticipated, the spinodal is defined by the two points of inflection of the $\beta\Delta\overline{G}$ curve that, in turn, are found to coincide with the minima of $\Delta g_{0,\alpha}$ and $\Delta g_{0,\beta}$. Furthermore, $\Delta g_{0,\alpha}$ and $\Delta g_{0,\beta}$ are identically nil at the boundary of the metastable region, i.e. at $\xi^{(0)} = \pm\ \xi$. Therefore, out of the spinodes the nucleation of only one of the two phases is permitted, this depending on the initial composition of the solid solution (Fig. 6). To be specific, for $\xi_{A,F} < \xi^{(0)} < \xi$ nucleation and growth of the $\beta$-phase is allowed since $\Delta g_{0,\beta} < 0$ and $\Delta g_{0,\alpha} > 0$ in this interval of composition. On the contrary, for $-\xi < \xi^{(0)} < -\xi_{A,F}$ the inequalities $\Delta g_{0,\alpha} < 0$ and $\Delta g_{0,\beta} > 0$ hold, which entails nucleation and growth of the α-phase. As far as the supersaturation is concerned, it is given by $\sigma_\alpha = \frac{x_A^{(0)} - x_A^{(\beta)}}{x_A^{(\alpha)} - x_A^{(\beta)}} = \frac{1}{2}\left(1 + \frac{\xi^{(0)}}{\xi}\right)$ or $\sigma_\beta = \frac{x_A^{(0)} - x_A^{(\alpha)}}{x_A^{(\beta)} - x_A^{(\alpha)}} = \frac{1}{2}\left(1 - \frac{\xi^{(0)}}{\xi}\right)$ and its maximum value, at a given $\xi$ (i.e. at a given $\beta\omega$), is equal to $\sigma_{\max}(\xi) = \frac{1}{2}\left(1 - \frac{\xi_{A,F}}{\xi}\right) = \frac{1}{2}\left(1 - \frac{1}{2\xi}\sqrt{1 - \frac{4\xi}{\ln\frac{1+2\xi}{1-2\xi}}}\right)$. In the range $0 < \xi < 1/2$, $\sigma_{\max}$ is therefore lower than $\lim_{\xi\to 0}\sigma_{\max}(\xi) = \frac{1}{2}(1 - 3^{-1/2}) \cong 0.21$ as displayed in Fig. 7. This computation shows that for the regular solution model considered here, the nucleation process occurs for $\sigma < 0.21$.

We are now in a position to evaluate the nucleation rate on the basis of the classical nucleation theory. In this approach, nucleus formation is thought to proceed by the attachment of monomers according to the reaction chain: $\ldots \underset{\leftarrow}{\overset{\rightarrow}{M_i}} + M_1 \underset{\leftarrow}{\overset{\rightarrow}{M_{i+1}}} + M_1 \underset{\leftarrow}{\overset{\rightarrow}{\ldots}}$ where $M_1$ denotes the monomer and $M_i$ a cluster made up of $i$ monomers. The steady state nucleation rate, per unit volume of the untransformed phase, is given by [35]

$$I = K^* Z n_1 e^{-\beta\Delta G^*}, \tag{15}$$

where $\Delta G^*$ is the free energy for critical nucleus formation, $Z$ the Zeldovich factor, $n_1$ the concentration of monomers and $K^*$ the rate constant of the process $M_{i^*} + M_1 \overset{K^*}{\rightarrow} M_{i^*+1}$, $i^*$ being the size of the critical nucleus. In Eq. 15, $\Delta G^* = \left(\frac{b}{3}\right)^3\left(\frac{2}{\Delta\mu}\right)^2, b = (36\pi/\rho_n^2)^{1/3}\gamma$, where $\rho_n$ and $\gamma$ are the density and the surface energy of the nucleus, respectively, and $i^*\Delta\mu$ is the bulk contribution to the free energy of nucleation. It is worth noting that in the case of one-component systems, application of Eq. 15 is straightforward. On the other hand, in order to employ Eq. 15 to deal with

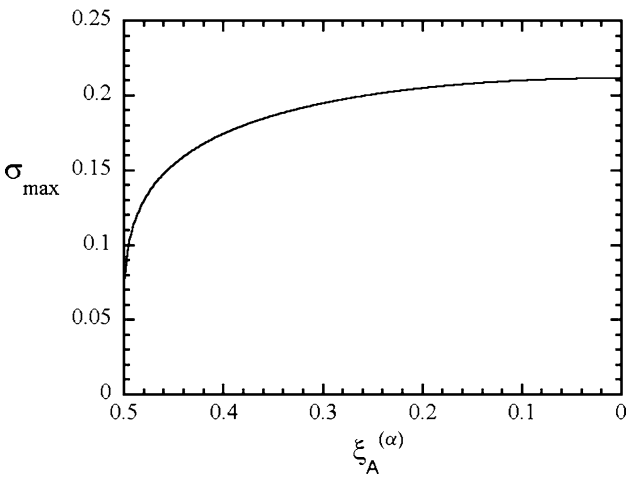


**Fig. 7** Maximum value of the supersaturation as a function of $\xi_A^{(\alpha)}$. The $\xi_A^{(\alpha)}$ quantity $(0 < \xi_A^{(\alpha)} < \frac{1}{2})$ characterizes the energetics of the alloy through the $\beta\omega(\xi_A^{(\alpha)})$ function

two-component systems, the concentration of the "monomer" has to be estimated. To this end, and with reference to the nucleation of the α-phase, one formally identifies the monomer with the $M_1 \equiv A_{x_A^{(\alpha)}} B_{x_B^{(\alpha)}}$ unit. Consequently, by denoting with $N_1$ the number of atoms available to be transferred into the α-phase, with $N_0$ the total number of atoms and with $\rho_0$ the density of the alloy, one gets $n_1 = \frac{N_1}{N_0}\rho_0$. On the other hand, since $N_1$ is also equal to the number of atoms transferred into the α-phase at the end of the transformation, use of the lever rule eventually leads to the relationship $n_1 = \rho_0\sigma_\alpha$. In addition, $K^* = \nu a_0 S^* c_A^{(0)}$ where $\nu$ and $a_0$ are the jump frequency and jump length of the atom, respectively, $S^*$ the surface area of the critical nucleus, and $c_A^{(0)}$ the concentration of the component in the parent-phase. The steady state nucleation rate, Eq. 15, becomes

$$I = \rho_0 \nu a_0 S^* Z c_A^{(0)} \sigma_\alpha e^{-\beta \Delta G^*}, \tag{16}$$

with $\Delta G^* = \left(\frac{b}{3}\right)^3 \left(\frac{2}{\Delta g_{0,\alpha}}\right)^2$, $b = (36\pi/\rho_\alpha^2)^{1/3}\gamma_{0,\alpha}$, where $\rho_\alpha$ and $\gamma_{0,\alpha}$ are the density and the interfacial energy, respectively. Besides, the Zeldovich factor is a function of the free energy of nucleation according to $Z = \frac{1}{9\Delta G^*}\left(\frac{\beta b^3}{\pi}\right)^{1/2}$. For the sake of simplicity in the following, the density is taken to be the same for all phases and will be denoted as $\rho_0$. Notably, $c_A^{(0)}$ and $b$ (and therefore $\Delta G^*$) are both functions of supersaturation or, alternatively, of the fraction of the transformed phase. Specifically, $c_A^{(0)} = \rho_0 x_A^{(0)} = \rho_0\left(\frac{1}{2} + \xi^{(0)}\right) = \rho_0\left(\frac{1}{2} + \xi(2\sigma_\alpha - 1)\right)$, which can be further expressed in terms of the transformed volume through Eq. 3. The nucleation rate is eventually given by

$$I(\sigma) = \kappa\rho_0 \nu \overline{\gamma}^{1/6}\left(\frac{1}{2} + \xi(2\sigma - 1)\right)\sigma \exp\left[-\overline{\gamma}/\left(\beta\Delta g_{0,\alpha}\right)^2\right], \tag{17}$$

where $\sigma \equiv \sigma_\alpha$, $\overline{\gamma} = \frac{16}{3}\pi\frac{(\beta\gamma_{0,\alpha})^3}{\rho_0^2}$ and $\kappa$ is a numerical factor of order of unity (with $a_0 \cong \rho_0^{-1/3}$). The surface energy, $\gamma_{0,\alpha}$, can be estimated by resorting to the Born–Stern broken-bond method by considering nearest neighbor interactions [35]. By retaining in the $\omega$ expansion only the contribution of the first coordination shell, one gets

$$\gamma_{0,\alpha} = \frac{\omega}{a z_1}(\xi - \xi^{(0)})^2, \tag{18}$$

where $a$ is the area occupied by one atom in the interface. By making use of Eq. 10, the $\overline{\gamma}$ term is eventually estimated as

$$\begin{aligned}\overline{\gamma} &= \frac{16}{3}\pi\left(\frac{\beta\omega}{z_1}\right)^3(\xi - \xi^{(0)})^6 \\ &= \frac{2}{3}\pi\left(\frac{1}{z_1\xi}\ln\frac{1+2\xi}{1-2\xi}\right)^3(\xi - \xi^{(0)})^6.\end{aligned} \tag{19}$$

where $a \cong \rho_0^{-2/3}$ was assumed.

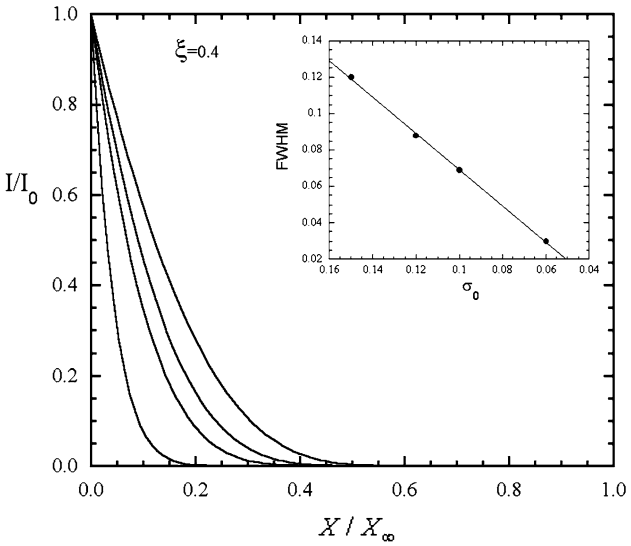


**Fig. 8** Steady state nucleation rate, according to the classical nucleation theory, as a function of $X/X_\infty$ for $z_1 = 6$, $\xi = 0.4$ and several values of $\sigma_0$: 0.06, 0.1, 0.12, and 0.15. The FWHMs of the normalized nucleation rates are displayed in the inset

Nucleation rates have been computed by means of Eqs. 17 and 19 for several values of the initial supersaturation subjected to the constraint $\sigma_0 < \sigma_{\max}(\xi)$. The normalized nucleation rate, $I(\sigma)/I(\sigma_0)$ versus $X/X_\infty$, computed for $z_1 = 6$ and $\xi = 0.4$, has been displayed in Fig. 8 and implies, according to Fig. 7, a maximum value of the supersaturation of about 0.17. From Fig. 8 one appreciates that the nucleation of all nuclei can be considered simultaneous the lower the supersaturation value. This behavior can be better analyzed by plotting the full width at half maximum (FWMH) of the normalized nucleation rate versus the initial supersaturation, as displayed in the inset of the same figure. The nucleation process can be assumed to reach completion for a volumetric fraction of the transformed phase of the order of 0.1–0.2.

It is worth noting, in passing, that the composition variable here employed allows us to study various situations. In particular, for a given $\xi$ the computation reported above holds for several values of the critical temperature of the alloy, $T_c$. In fact, from Eq. 10 it follows that $T_c = T\frac{1}{4\xi}\ln\frac{1+2\xi}{1-2\xi}$ and thus depends on temperature. In the limit $\xi \to 0$ one gets $T \to T_c$ and the phase separation does not occur.

## The thermodynamic factor

So far Fick's law has been employed by considering the diffusion coefficient to be independent of concentration. In other words, the thermodynamic factor has been taken equal to one. In this section, we briefly analyze the validity of this assumption in the framework of the regular solution

model discussed in the previous section, which allows for a straightforward determination of the activity coefficient. For component $A$, the generalized transport equation is $J_A = -\beta D_A \frac{\partial \mu_A}{\partial \ln c_A} \nabla c_A$ and the thermodynamic factor is estimated by means of Eq. 11a according to

$$\beta \frac{\partial \mu_A}{\partial \ln c_A} = 1 - 2\beta\omega x_A(1 - x_A), \tag{20}$$

where $x_A = \frac{c_A}{\rho_0}$ is the mole fraction of the component. It follows that Eq. 2a holds provided $2\beta\omega x_A x_B$ is much lower than unity.

The plot of $2\beta\omega x_A x_B$ as a function of supersaturation is displayed in Fig. 9 for various values of $\xi$ in the range 0.1–0.45. In these computations, the supersaturation is lower than the $\sigma_{\max}(\xi)$ function reported in Fig. 7. From Fig. 9 it stems that in the low supersaturation regime the thermodynamic factor can be taken equal to one provided $\xi$ is sufficiently large. Furthermore, although for small $\xi$ the thermodynamic factor is not negligible, it is found to depend weakly on supersaturation and this validates the use of Fick's law.

In the region of the phase diagram where nucleation is thermally activated, the maximum value of $2\beta\omega x_A x_B$ is obtained at the inflection points, namely at $\xi^{(0)} = \pm\xi_{A,F}$, according to $2\beta\omega\left(\frac{1}{4} - \xi_{A,F}^2\right) = 1$. This is the value reached by the curves of Fig. 9 for $\sigma/\sigma_{\max}(\xi) = 1$, where $\sigma_{\max}(\xi) = \frac{1}{2}\left(1 - \frac{\xi_{A,F}}{\xi}\right)$.

## Effect of the nucleus curvature on interface composition

In this section, we study the effect of the curvature of the nucleus on the composition of the interface. The solid solution is thought to be regular and the formation of α-nuclei is assumed. This analysis is useful in order to give an assessment of the approximation employed in section "Simultaneous nucleation" regarding the Gibbs–Thomson effect. To this aim, the excess free energy of the interface has to be taken into account in the expression of the free energy of the system,

$$G = n_A^{(\alpha)}\mu_A^{(\alpha)} + n_A^{(\beta)}\mu_A^{(\beta)} + n_B^{(\alpha)}\mu_B^{(\alpha)} + n_B^{(\beta)}\mu_B^{(\beta)} + 4\pi R_\alpha^2 \gamma_{0,\alpha}, \tag{21}$$

where $n$ stands for the composition variable and the chemical potentials are given by Eqs. 11a and 11b. To simplify the notation in the following, $\gamma \equiv \gamma_{0,\alpha}$ and $R \equiv R_\alpha$ are used. From Eq. 21 one derives the equilibrium condition between the two phases according to

$$\begin{cases} \mu_A^{(\alpha)} + \frac{2\gamma\overline{v}_A^{(\alpha)}}{R} = \mu_A^{(\beta)} \\ \mu_B^{(\alpha)} + \frac{2\gamma\overline{v}_B^{(\alpha)}}{R} = \mu_B^{(\beta)}, \end{cases} \tag{22}$$

where $\overline{v}_A^{(\alpha)}$ and $\overline{v}_A^{(\beta)}$ are the partial molar volumes of $A$ and $B$ in the α-phase nucleus. Equation 22 is a system in the two unknowns, $x_A^{(\alpha)}(R)$ and $x_A^{(\beta)}(R)$, which are the two independent variables of composition, both functions of $R$. These two equations lead to the common tangent construction in the Gibbs free energy diagram where $\overline{G}^{(\alpha)}(R) = \overline{G}^{(\alpha)}(\infty) + \frac{2\gamma\overline{V}^{(\alpha)}}{R}$, $\overline{V}^{(\alpha)}$ is the molar volume of the α-phase and $\overline{G}^{(\alpha)}(\infty)$ the free energy of the planar interface [36]. A discussion on the application of the common tangent approach to solid–solid system has been reported in Ref. [36] and references therein.

In order to check the validity of the approximation employed in the model kinetics, the system Eq. 22 is solved by considering small deviations in the compositions from the values proper of the planar interface, which are referred to, in this section, as $x_A^{(\alpha)}(\infty)$ and $x_A^{(\beta)}(\infty)$. These values are in accord with the phase diagram and correspond to the variables $x_A^{(\alpha)}$ and $x_A^{(\beta)}$ defined in the previous sections (Fig. 1b). Accordingly, one gets

$$\mu_A\left(x_A^{(\alpha)}(R)\right) \cong \mu_A\left(x_A^{(\alpha)}(\infty)\right) + \left(\frac{\partial \mu_A}{\partial x_A}\right)_{x_A^{(\alpha)}(\infty)} \Delta x_A^{(\alpha)} \tag{23a}$$

$$\mu_A\left(x_A^{(\beta)}(R)\right) \cong \mu_A\left(x_A^{(\beta)}(\infty)\right) + \left(\frac{\partial \mu_A}{\partial x_A}\right)_{x_A^{(\beta)}(\infty)} \Delta x_A^{(\beta)}, \tag{23b}$$

where $\Delta x_A^{(\alpha)}$ and $\Delta x_A^{(\beta)}$ are the deviations from the compositions of the planar interface. The system then becomes

$$\begin{cases} \left(\frac{\partial \mu_A}{\partial x_A}\right)_{x_A^{(\alpha)}(\infty)} \Delta x_A^{(\alpha)} + \frac{2\gamma\overline{v}_A^{(\alpha)}}{R} \cong \left(\frac{\partial \mu_A}{\partial x_A}\right)_{x_A^{(\beta)}(\infty)} \Delta x_A^{(\beta)} \\ \left(\frac{\partial \mu_B}{\partial x_A}\right)_{x_A^{(\alpha)}(\infty)} \Delta x_A^{(\alpha)} + \frac{2\gamma\overline{v}_B^{(\alpha)}}{R} \cong \left(\frac{\partial \mu_B}{\partial x_A}\right)_{x_A^{(\beta)}(\infty)} \Delta x_A^{(\beta)} \end{cases} \tag{24}$$

where $\left(\frac{\partial \mu_A}{\partial x_A}\right) = (1 - x_A)\frac{\partial^2 \Delta\overline{G}}{\partial x_A^2}$, $\left(\frac{\partial \mu_B}{\partial x_A}\right) = -x_A \frac{\partial^2 \Delta\overline{G}}{\partial x_A^2}$ and $\Delta\overline{G}$ is given by Eq. 9. By specifying $\overline{v} = \rho_0^{-1}$ in Eq. 24, the solution

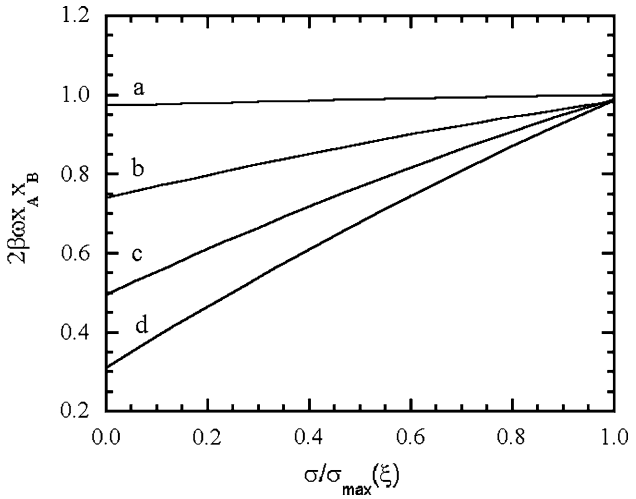


**Fig. 9** Thermodynamic factor in the framework of the regular solution model. Plot of the function $2\beta\omega x_A x_B$ as a function of normalized supersaturation, $\sigma/\sigma_{\max}(\xi)$, for several values of $\xi \equiv \xi_A^{(\alpha)}$: (a) $\xi = 0.1$, (b) $\xi = 0.3$, (c) $\xi = 0.4$, and (d) $\xi = 0.45$

of the system can be expressed in terms of the quantity $\xi \equiv \xi_A^{(\alpha)} = x_A^{(\alpha)}(\infty) - \frac{1}{2}$ defined above. The result reads,

$$\Delta x_A^{(\alpha)} = \Delta x_A^{(\beta)} = \frac{\beta\gamma\left(1-4\xi^2\right)}{2\rho_0 R\xi\left[2-\beta\omega\left(1-4\xi^2\right)\right]} \tag{25}$$

where, according to Eq. 10, $\beta\omega$ is a function of $\xi$. It is worth recalling that in this computation $\xi$ refers to the equilibrium composition, for a planar interface, of component $A$ in the $\alpha$-phase, where $\xi > 0$ has been assumed (Fig. 1b). The supersaturation is eventually estimated as

$$\begin{aligned}\psi &= \frac{c_A^{(0)} - c_A^{(\beta)}(\infty) - \rho_0 \Delta x_A^{(\beta)}}{c_A^{(\alpha)}(\infty) - c_A^{(\beta)}(\infty) + \rho_0\left(\Delta x_A^{(\alpha)} - \Delta x_A^{(\beta)}\right)} \\ &= \sigma - \frac{\Delta x_A^{(\beta)}}{2\xi},\end{aligned} \tag{26}$$

where $x_A^{(\alpha)} - x_A^{(\beta)} = 2\xi$ and $c = \rho_0 x$ was used. In the limit $\Delta x_A^{(\beta)} \ll 2\xi$, the supersaturation approaches $\sigma$, which is the value employed in section "Simultaneous nucleation". Moreover, since $\Delta x_A^{(\beta)} > 0$, the actual supersaturation is always lower than that which applies for the planar interface. It is worth noting that performing the computation above in terms of the $x_B$ variable, the expected result $\Delta x_B^{(\alpha)} = -\Delta x_A^{(\alpha)}$ is obtained.

Equation 26 is the basic equation for dealing with the effect of the nucleus curvature on the kinetics of the phase separation. In fact, with reference to the system of rate equations, Eqs. 4a–c, the nucleus curvature entails a change in the rate equation for the supersaturation (Eq. 4b). As reported in the Appendix, this last equation has to be recalculated, by using Eq. 26, and by taking into account the time dependence of the nucleus radius, $R(t)$, in the $\Delta x_A^{(\beta)}$ expression. The uncertainty arising from the assumption of planar interface can be analyzed, quantitatively, by comparing the $\psi$ and $\sigma$ quantities. By making use of Eq. 26, the expression of the volumetric fraction of the transformed phase, namely $X(t) = \frac{c_A^{(0)}(t=0) - c_A^{(0)}(t)}{c_A^{(\alpha)}(R(t)) - c_A^{(0)}(t)}$, can be recast in the form

$$X = \left(\sigma_0 - \frac{\Delta x_A^{(\beta)}}{2\xi} - \psi\right)\frac{1}{1-\psi}, \tag{27}$$

where $\sigma_0 \equiv \sigma(0) = \frac{x_A^{(0)}(t=0) - x_A^{(\beta)}(\infty)}{x_A^{(\alpha)}(\infty) - x_A^{(\beta)}(\infty)}$ is the initial supersaturation for a planar interface. By specifying Eq. 25 in Eq. 27 and employing the KJMA equation for the simultaneous nucleation case (Eq. 4c), one eventually gets the supersaturation as a function of $X$

$$\psi = \left(\sigma_0 - \frac{\beta\gamma a_0^2(1-4\xi^2)x_N^{1/3}}{4\xi^2\overline{\omega}\rho} - X\right)\frac{1}{1-X}, \tag{28}$$

to be compared with the supersaturation in the case of a planar interface, $\sigma = \frac{\sigma_0 - X}{1-X}$. In Eq. 28 $\overline{\omega} = 2 - \beta\omega(1-4\xi^2)$, $\rho = \left(\frac{3}{4\pi}\ln\frac{1}{1-X}\right)^{1/3}$, $x_N = \left(\frac{a_0}{d}\right)^3$ and $a_0 = \rho_0^{-1/3}$. Moreover, Eqs. 25 and 26 show that the nucleus size has to be sufficiently large to ensure $\psi > 0$. This condition is satisfied provided $2\xi\sigma > \Delta x_A^{(\beta)}$, that is $\frac{\beta\gamma(1-4\xi^2)}{4\rho_0\sigma\xi^2\overline{\omega}R} < 1$. Since this inequality also has to be verified for the smallest values of $R$, i.e. the critical radius $R^* = \frac{2\gamma}{\rho_0\left|\Delta g_{0,\alpha}\right|}$, one ends up with

$$\frac{\beta\left|\Delta g_{0,\alpha}\right|(1-4\xi^2)}{8\sigma_0\overline{\omega}\xi^2} < 1. \tag{29}$$

This inequality is found to be fulfilled for $\sigma_0 = \sigma_{\max}(\xi)$ in the whole $\xi$ domain. The $x_N$ value is also subjected to a constraint. In fact, the volume occupied by critical clusters (at the beginning of the transition) has to be much lower than the volume of the nuclei at the end of the transformation, and this implies $x_N \ll \sigma_0/i^*$.

The behavior of the supersaturation as a function of transformed volume (Eq. 28) has been shown in Fig. 10A and B for several values of the nucleation densities at $\xi = 0.4$, $\xi = 0.25$ and $\sigma_0 = \sigma_{\max}(\xi)$. In fact, the inequality above is fulfilled for $x_N$ much lower than $10^{-3}$ and $10^{-4}$ for $\xi = 0.4$ and $\xi = 0.25$, respectively. In these computations, the maximum value of the surface free energy has been used, and is that obtained for $\xi^{(0)} = -\xi$. Comparison with the supersaturation of planar interface, also shown in the same panel, indicates that the effect of nucleus curvature becomes more important the larger the nucleation density, the smaller the fraction of transformed phase and the smaller the $\beta\omega = 2T_c/T$ quantity. Besides, the finite curvature of the nucleus entails a decrease of supersaturation when compared to that which applies for a planar interface, in the whole range of transformed volume. This affects the value of the volumetric fraction at the end of the transition, i.e. for $\psi \to 0$, that is now lower than $\sigma_0$ (Fig. 10).

The characteristic length, $\eta$, has also been investigated by taking into account the impact of the nucleus curvature on interface composition. The details of the computation are reported in the Appendix. It is found that the behavior of the ratio $\rho/\eta$ with the volumetric fraction is very similar to that obtained through Eq. 6 for planar interface. The computation shows that the relative deviation of $\rho/\eta$ from Eq. 6 is of the order of a few percent in the whole range of the transformed volume (Fig. 11). Finally, we report on the kinetics of the transformed volume by considering the Gibbs–Thomson effect. For this purpose, knowledge of the $\rho/\eta$ function is required, for it enters the rate equation for the volumetric fraction Eq. A10. This equation has been numerically integrated for the same values of the parameters as in Fig. 11 and the results have been displayed in Fig. 12. As it appears, consideration of the Gibbs–Thomson effect leads to a slowing down of the kinetics, to an extent that depends on nucleus density, and to a decrease of

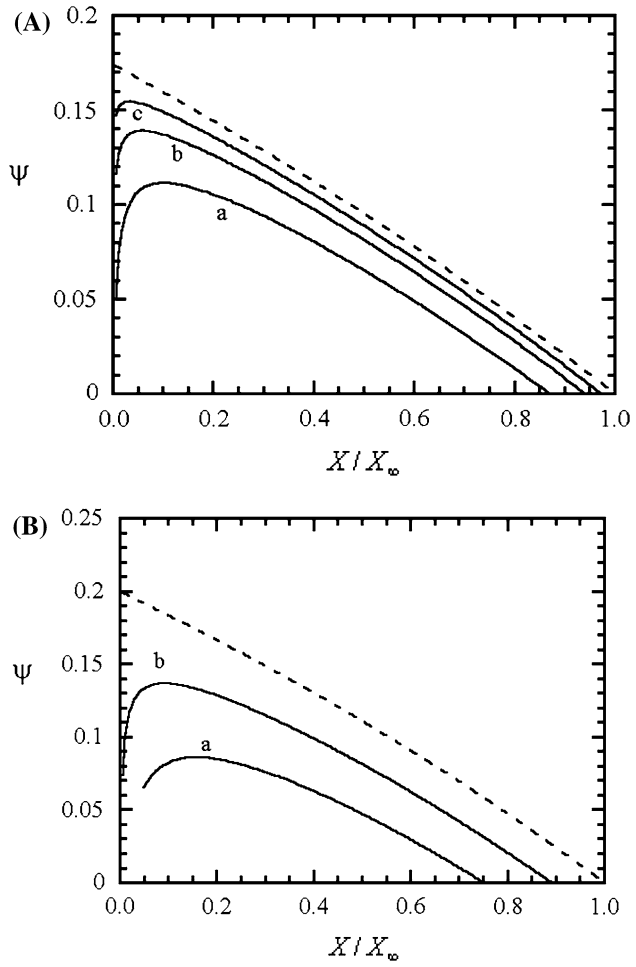


**Fig. 10** Effect of nucleus curvature on interface composition. The supersaturation is shown as a function of transformed volume for $\xi = 0.4$ and $\xi = 0.25$ in **A** and **B**, respectively, and for several values of the nucleation density. In the abscissa, the fraction of transformed volume is normalized to $X_\infty = \sigma_0 = \sigma_{\max}(\xi)$. **A** $x_N = 10^{-4}$ (curve a), $x_N = 10^{-5}$ (curve b), and $x_N = 10^{-6}$ (curve c). **B** $x_N = 10^{-5}$ (curve a) and $x_N = 10^{-6}$ (curve b). In curve (a) of **B**, the computation holds for volume fraction greater than $X^*/\sigma_0 \cong 0.05$. The supersaturation in the case of planar interface is also displayed as *dashed line*

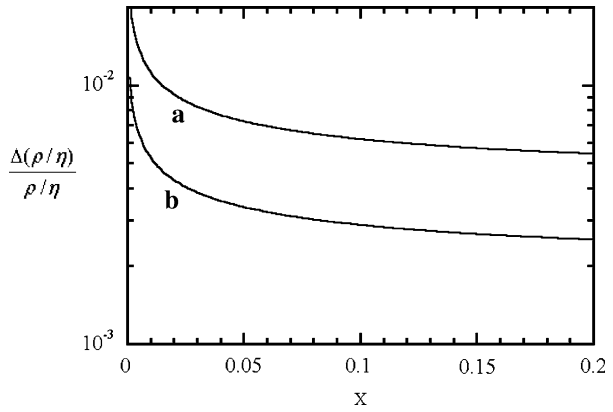


**Fig. 11** Relative variation of $\rho/\eta$ from the value obtained neglecting the Gibbs–Thomson effect (Eq. 6). The computation has been performed for $\xi = 0.4$ and $\sigma_0 = \sigma_{\max}(\xi)$. (a) $x_N = 10^{-5}$ and (b) $x_N = 10^{-6}$

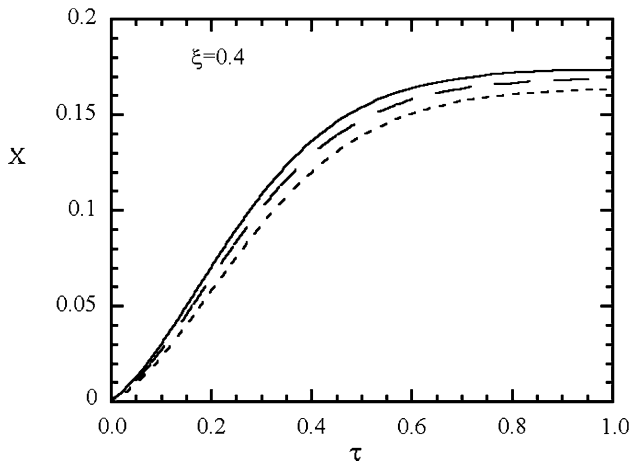


**Fig. 12** Kinetics of the transformed volume by considering the effect of nucleus curvature on interface composition. As in Fig. 11 computations refer to the case $\xi = 0.4$ and $\sigma_0 = \sigma_{\max}(\xi)$. (*Dashed line*) $x_N = 10^{-5}$; (*long dashed line*) $x_N = 10^{-6}$. The kinetics computed in the limit of planar interface is also reported as *full line*

the final value of the transformed volume. Finally, it is worth recalling that these results are correct within the linear approximation exploited in Eq. 24.

## Conclusion

A model kinetics has been presented for describing solid–solid phase transition, ruled by nucleation and growth processes, in binary alloys. The model relies on a system of mean field rate equations where the characteristic distance, $y$, depends on nucleus radius and diffusion length, both functions of time. The time dependence of the supersaturation is related to the diffusion length of the atoms. In the case of simultaneous nucleation, the duration of the transformation exhibits a power dependence on the diffusion coefficient, nucleation density, and initial supersaturation. The analysis of the nucleation process, based on the regular solution approach, shows that the nucleation can be considered, approximately, as simultaneous. Under these circumstances, Ham's equation is well verified. In addition, for low values of either $\xi$ or $\sigma$, Fick's law is suitable for describing the growth process. The impact of the nucleus curvature on interface composition has also been analyzed. It is found that this effect is relevant in the case of high nucleation density and low values of the transformed volume. Moreover, the Gibbs–Thomson effect implies a decrease of the transformed volume at the end of the phase separation when compared to the one computed for a planar interface.

**Acknowledgement** The author is grateful to Dr. N. Downer for the critical reading of the manuscript.

## Appendix

This appendix is devoted to computing the rate equations for both supersaturation ($\psi$) and fraction of transformed volume ($X$), by taking into account the Gibbs–Thomson effect discussed in section "Effect of the nucleus curvature on interface composition". From the definition $\psi = \frac{c_A^{(0)} - c_A^{(\beta)}}{c_A^{(\alpha)} - c_A^{(\beta)}}$ one obtains

$$c_A^{(0)} = \rho_0(2\xi\psi + x_A^{(\beta)}(\infty) + \Delta x_A^{(\beta)}), \tag{A1}$$

where Eq. 25 was used. Also, the rate equation for $c_A^{(0)}$ reads

$$\frac{\mathrm{d}c_A^{(0)}}{\mathrm{d}\tau} = -\frac{1}{\eta^2}\left(c_A^{(0)} - c_A^{(\beta)}\right) = -\frac{2\rho_0\xi\psi}{\eta^2}. \tag{A2}$$

By equating the time derivative of Eq. A1 to Eq. A2, the changing rate of the supersaturation is obtained according to

$$\frac{\mathrm{d}\psi}{\mathrm{d}\tau} = -\frac{\psi}{\eta^2} + \frac{\Delta x_A^{(\beta)}}{2\xi}\frac{\mathrm{d}\ln\rho}{\mathrm{d}\tau}, \tag{A3}$$

where $\frac{\mathrm{d}\ln\Delta x_A^{(\beta)}}{\mathrm{d}\tau} = -\frac{\mathrm{d}\ln\rho}{\mathrm{d}\tau}$ was employed (Eq. 25). Equation A3, together with Eq. 4a, i.e. $\frac{\mathrm{d}\rho}{\mathrm{d}\tau} = \psi\left(\frac{1}{\rho} + \frac{1}{\eta}\right)$, allows one to evaluate the characteristic length. In fact, the equalities hold,

$$\frac{\mathrm{d}\rho}{\mathrm{d}\psi} = \frac{\frac{\mathrm{d}\rho}{\mathrm{d}\tau}}{\frac{\mathrm{d}\psi}{\mathrm{d}\tau}} = \frac{\psi\left(\frac{1}{\rho} + \frac{1}{\eta}\right)}{-\frac{\psi}{\eta^2} + \frac{K_0}{2\xi\rho}\frac{\mathrm{d}\ln\rho}{\mathrm{d}\tau}}, \tag{A4}$$

where $K_0 = \Delta x_A^{(\beta)}\rho$. On the other hand, the derivative of the KJMA formula, $\rho = \left(\frac{3}{4\pi}\ln\frac{1}{1-X}\right)^{1/3}$, is

$$\frac{\mathrm{d}\rho}{\mathrm{d}\psi} = \frac{1}{4\pi\rho^2}\frac{1}{(1-X)}\left(\frac{\mathrm{d}\psi}{\mathrm{d}X}\right)^{-1}, \tag{A5}$$

where, according to Eq. 28,

$$\psi = \left(\sigma_0 - \frac{K_0}{2\xi\rho} - X\right)\frac{1}{1-X}. \tag{A6}$$

The equality between Eqs. A4 and A5 gives

$$\psi\left(\frac{1}{\rho} + \frac{1}{\eta}\right) = \left[-\frac{\psi}{\eta^2} + \frac{K_0}{2\xi\rho^2}\psi\left(\frac{1}{\rho} + \frac{1}{\eta}\right)\right]\frac{1}{4\pi\rho^2(1-X)}\left(\frac{\mathrm{d}\psi}{\mathrm{d}X}\right)^{-1}, \tag{A7}$$

that eventually leads to the following second order equation for $\eta(X)$:

$$\eta^{-2} - \chi(\eta^{-1} + \rho^{-1}) = 0, \tag{A8}$$

where $\chi = 4\pi\rho^2\left(\frac{1-\sigma_0}{1-X}\right) - \frac{K_0}{2\xi(1-X)}\left(\frac{X}{\rho^2} - 4\pi\rho\right)$. In the limit of planar interface $K_0 = 0$ and the solution of Eq. A8 reduces to Eq. 6 with $X = \frac{\sigma_0 - \sigma}{1-\sigma}$.

The rate equation for $X(\tau)$ is obtained by equating the growth rate of the nucleus, as given by the KJMA kinetics, to Eq. 4a. Specifically,

$$\frac{\mathrm{d}\rho}{\mathrm{d}\tau} = \left[4\pi\rho^2(1-X)\right]^{-1}\frac{\mathrm{d}X}{\mathrm{d}\tau} = \frac{\psi}{\rho}\left(1 + \frac{\rho}{\eta}\right) \tag{A9}$$

which leads to

$$\frac{\mathrm{d}X}{\mathrm{d}\tau} = \left(\sigma_0 - \frac{K_0}{2\xi\rho} - X\right)\left(1 + \frac{\rho}{\eta}\right)4\pi\rho, \tag{A10}$$

where the $\psi(X)$ expression was used (Eq. A6). In fact, the right-hand side member of Eq. A10 is a function of $X$ since $\rho(X)$ is given by the KJMA formula and $\eta(X)$ by solving Eq. A8.

## References


1. Kolmogorov AN (1937) Bull Acad Sci URSS (Cl Sci Math Nat) 3:355
2. Johnson WA, Mehl RF (1939) Trans Am Inst Min Metall Pet Eng 135:416
3. Avrami M (1939) J Chem Phys 7:1103
4. Avrami M (1940) J Chem Phys 8:212
5. Zener C (1949) J Appl Phys 21:950
6. Hermann H, Mattern N, Roth S, Uebele P (1997) Phys Rev B 56:13888
7. Svoboda J, Fischer FD, Fratzl P, Gamsjäger E, Simha NK (2001) Acta Mater 49:1249
8. Nagase T, Yamauchi I, Ohnaka I (2001) J Alloys Compd 316:212
9. Schmidt U, Schmidt B (2000) Mater Sci Forum 331:889
10. Starink MJ, Zahra A-M (1999) J Mater Sci 34:1117
11. Starink MJ (2004) Int Mater Rev 49:191
12. Fanfoni M, Tomellini M, Volpe M (2002) Phys Rev B 65:172301
13. Rios PR, Oliveira JCPT, Oliveira VT, Castro JA (2006) Mater Res 9:165
14. Birnie DP III, Weinberg MC (1995) J Chem Phys 103:3742
15. Burbelko AA, Fraś E, Kapturkiewicz W (2005) Mater Sci Eng A 413:429
16. Shepilov MP, Baik BS (1994) J Non-Cryst Solids 171:141
17. Shepilov MP (2004) Glass Phys Chem 30:291
18. Farjas J, Roura P (2007) Phys Rev B 75:184112
19. Pusztai T, Gránásy L (1998) Phys Rev B 57:14110
20. Kooi BJ (2004) Phys Rev B 70:224108
21. Bruna P, Crespo D, Gonzalez-Cinca R (2006) J Appl Phys 100:054907
22. Pradell T, Crespo D, Clavaguera N, Clavaguera-Mora MT (1998) J Phys Condens Matter 10:3833
23. Zhao J, Li H, Wang Q, He J (2008) Comput Mater Sci. doi:10.1016/j.commatsci.2008.03.037
24. Zhao J, Li H, Zhang X, He J (2008) Mater Lett 62:3779
25. Tomellini M (2003) J Alloys Compd 348:189
26. Bales GS, Chrzan DC (1994) Phys Rev B 50:6057
27. Grabke HJ (1998) Mater Corr 49:303
28. Grabke HJ (2003) Mater Corr 54:736

29. Szakálos P (2003) Mater Corr 10:54
30. Hillert M (1999) Acta Mater 47:4181
31. Raghavan V, Cohen M (1975) In: Bruce Hannay N (ed) Treatise on solid state chemistry, vol 5, chap 2. Plenum Press, New York, p 67
32. Pineda E, Crespo D (2003) J Non-Cryst Solids 317:85
33. Ham FS (1958) J Phys Chem Solids 6:335
34. Bulyarskii SV, Svetukhin VV, Agafonova OV, Grishin AG, Ilin PA (2002) Phys Status Solidi 231:237
35. Mutaftschiev B (2001) The atomistic nature of crystal growth. Springer-Verlag, Berlin
36. Qian M (2002) Metall Mater Trans A 33:1283